Supplemental Material for

Engineering Polarons at a Metal Oxide Surface

C. M. Yim,[1] M. B. Watkins,[2] M. J. Wolf,[3,4] C. L. Pang,[1] K. Hermansson,[4] and G. Thornton[1]

[1] *Department of Chemistry and London Centre for Nanotechnology, University College London, 20 Gordon Street, London, WC1H 0AJ, UK*

[2] *School of Mathematics and Physics, University of Lincoln, Brayford Pool, Lincoln LN6 7TS UK*

[3] *Department of Physics & Astronomy and London Centre for Nanotechnology, University College London, Gower Street, London, WC1E 6BT, UK*

[4] *Department of Chemistry – Ångström Laboratory, Uppsala University, Box 538, S-751 21 Uppsala, Sweden*

Experimental Details

Scanning Tunnelling Microscopy (STM) experiments were performed using an *Omicron GmbH* low temperature ultrahigh vacuum (UHV) STM [1]. In order to identify O_b-vacs, and probe the excess electrons associated with them, we recorded filled- and empty-state STM quasi-simultaneously. This was achieved in the following way: In the forward scan in the fast direction, a line of data is recorded at positive sample bias, and in the backward scan a line of data is recorded with negative sample bias. This approach eliminates the effects of thermal or piezo drift so that scans with the opposite polarity are easily correlated. To rule out the introduction of features from the forward scan to the backward scan, we occasionally reversed the polarity, i.e. forward scans were performed with a negative bias voltage and backward scans with a positive bias. No differences were observed in the resulting images.

Sample preparation

As shown in fig. S1, we used a special three-step preparation procedure in order to obtain a sample sufficiently conductive at 7 K yet with O_b-vac well separated: (i) Fresh TiO_2(110) samples (*Pi-Kem*) were subjected to approximately ninety Ar^+ ion sputtering and annealing cycles up to ~1000 K. (ii) Such 'as-prepared' samples were left in the preparation chamber with a background pressure of 2×10^{-10} mbar at room temperature, where water from the residual vacuum reacts with O_b-vacs, forming two bridging hydroxyls (OH_b) for each O_b-vac [2-4]. In this way, a TiO_2 (110) surface is formed with a significant density of OH_b but very few O_b-vacs [2-4]. (iii) +3 V STM scans are applied

to a part of the surface, removing H from the OH_b but leaving in place the O_b-vac [3,5-7]. We verified that such +3 V scans do not alter the excess electron distributions around the O_b-vacs by comparing images recorded before and after the +3 V scans. We have tested the behavior of this surface via reaction with water and by scanning tunneling microscopy and spectroscopy. No unusual behavior compared to as-prepared surfaces was observed.

Selection of isolated O_b-vacs

To ensure that the images in Fig. 1 of the Letter are representative of isolated O_b-vacs in general, we sampled ~10 O_b-vacs that were not in close proximity either to other O_b-vacs or to positively charged subsurface impurity atoms [8,9]. These positively charged subsurface impurity atoms, which are suggested to be either intrinsic (Ti) or extrinsic interstitials (Mg, Fe, Si and Al) [9], can induce downward band bending [8], and hence are believed to distort the distributions of the excess electrons associated with the O_b-vacs that are located in their proximity. All of the sampled O_b-vacs produced images similar to those shown.

We also checked whether regions with high filled-states density interacted with each other by using the STM tip to push two O_b-vacs towards each other. When the O_b-vac polarons were separated from each other by at least three unit cells along the $[001]$ direction or one unit cell along the $[\bar{1}10]$ direction, no interaction was observed in the filled state image. We only consider isolated O_b-vacs that are separated from other bright features in the filled-state image by at least these distances.

Note that in the filled-state images presented in Fig. 1 and in other experimental images that are discussed in the Letter, we observed some regions of enhanced contrast that do not appear to be associated with O_b-vacs. We believe that they arise from subsurface species such as interstitial Ti [8]. Charged species as deep as five layers down in TiO_2(110) are thought to be detectable in STM [9]. On the basis that these additional bright regions arise from Ti interstitials distributed in the top five surface layers, our accumulated images give a mean density of 0.016 ML [where 1 ML (monolayer) is defined as the density of (1 × 1) unit cells, 5.2×10^{14} cm^{-2}], which is well below the upper limit reported for Ti interstitials in the top few layers of 0.05-0.07 ML [6,10].

Vacancy manipulation

In previous work, Minato *et al*. [11] applied +4 V pulses directly over an O_b-vac, which led to its displacement in a random direction. However, by applying a pulse (sample bias +4 V, 6 s) over an O_b^{2-} *adjacent* to an O_b-vac, we created an O_b-vac at a *targeted* O_b^{2-} site, with the original O_b-vac being healed, as shown in Movie S1. The displacement of the O_b-vac is presumably caused by the electric field at the tip: during the pulse, the negatively charged tip is placed over the negatively charged O_b^{2-} ion repelling it into the O_b-vac.

Calculation Details

The calculations reported in this paper were performed using the CP2K program suite. The Quickstep DFT module [12] was used to carry out localised basis-set hybrid density-functional calculations using the PBE0-TC-LRC-ADMM hybrid density

functional [13,14], containing 20% exact exchange. The exact exchange contribution was truncated at a distance of 0.2 nm and exchange at further distances approximated by an exchange-hole based on the underlying PBE functional. PBE0-TC-LRC-ADMM, in our experience, behaves very similarly to the screened HSE06 functional (notably the generalised Koopman's theorem is satisfied for polarons in bulk rutile TiO_2), but is significantly less expensive, allowing the calculations on large, electronically complex systems presented here to be performed. Even then, it has not been feasible for us to carry out exhaustive and systematic searches for the ground electronic states of the multiple vacancy defects, as the number of possible polaronic configurations grows combinatorially. It is also important to point out that we only consider static configurations of polarons here at DFT level, while the whole dynamics involving phonon-assisted polaron hopping would require *ab initio* molecular dynamics to begin to understand the full picture.

The primary basis set was of TZVP quality for Ti (based upon the DZVP-MOLOPT-SR-GTH basis distributed with the code [15]; see SI therein), and TZV2P for O with the corresponding GTH pseudo-potentials [16,17]. The auxiliary Gaussian basis for the ADMM method was pFIT3 as detailed in ref. [14] and a FIT3 basis for Ti was optimised using the procedure outlined in the same paper. Wave-function optimizations were performed using the orbital transformation method [18]. For STM image simulations additional spherical basis functions (with exponents 0.25, 0.1, 0.05 $bohr^{-2}$) were placed in the vacuum above the surface at the sites that would be occupied by atoms if the surface had not been cleaved, a procedure which has been shown to be able to reproduce simulated STM images calculated using a plane-wave basis [19].

The system consisted of 4 TiO_2 tri-layers, with the bottom two tri-layers fixed in position and capped with pseudo-hydrogen to give a clean band-gap in the surface system. The surface band-gap of the ideal system was found to be 3.0 eV as opposed to 3.2 eV in the bulk. We use 8×2 or 8×4 surface super-cells for CP2K calculations with dimensions 2.362 × 1.296 nm^2 or 2.362 × 2.592 nm^2 and 384 or 768 TiO_2 molecules. The CP2K DFT simulations use 2D periodic boundary conditions using the Poisson solver of Genovese *et al*. [20]. Transition state calculations to estimate reaction barriers used the climbing image nudged elastic band method [21] with 3 intermediate images.

Given the relative novelty of the ADMM method, we also wished to compare the simulated STM images generated with it to those calculated using the well established DFT+U method, as implemented in the plane-wave VASP code. This was done for the isolated vacancy only. These calculations used the projector augmented wave method to account for the core electrons, along with the PBE gradient corrected functional, and an effective U value of 3.5 eV. A 4 tri-layer slab was used, of which the bottom tri-layer was held fixed, with a 6×2 surface supercell. A cut-energy of 400 eV was used, with a 1×3×2 k-point mesh, which was generated automatically according to the Monkhorst-Pack scheme. As can be seen in Fig. S6, the two methods produce images that are in very good agreement.

Classical molecular dynamics (MD) calculations were used as an exploratory tool. Apparent minima and transition states discovered were fully reoptimized using DFT. Classical molecular dynamics calculations used the FIST module of CP2K and employed the shell-model [22] reparameterization of the Akaogi force-field [23] for rutile TiO_2 [24]. Cell dimensions were set to those of the CP2K DFT calculations to allow ready

transfer of geometries between the two force calculation methods. Molecular dynamics was performed at 77 K using the thermostat of Bussi *et al*. [25]; shells were given 0.2 of the mass of their corresponding cores and were separately thermostatted to 25 K. Classical molecular dynamic calculations are useful for providing insights on relevant configurations of the lattice and charge distributions. However, such parameterised approaches would necessarily have considerable limitations given the added complexity introduced by the increasing size of the mutlimer vacancy complexes, so all local minima, and suspected transition states linking them, were reoptimized at a DFT level. Only DFT energies are reported in the paper.

STM simulations

All STM image simulations were performed using the standard Tersoff-Hamman approximation [26] in the constant current (constant density of states at 1×10^{-7} electrons/Å^3) mode. Empty states images were generated including states up to ~0.5 eV above the lowest unoccupied Kohn-Sham orbitals. Filled state images included all states localised on Ti atoms that are within the band-gap of the ideal surface – 2 states for each removed oxygen atoms; 2 for the O vacancy, 4 for the O vacancy dimer, 6 for the trimer and 8 for the tetramer. As states due to the background of reduced sites in the crystal are not present, a constant background density of 1×10^{-7} electrons/Å^3 was introduced at 0.15 nm above the bridging oxygen rows. All simulated STM images were calculated using 2.59×2.36 nm^2 supercells.

For the complexes there are many electronic solutions available, corresponding to the different distributions of the electrons over subsurface Ti sites. No attempt has been

made to calculate all possible configurations, as this is beyond reasonable computational effort currently. Instead images were calculated from super-positions of the lowest few electronic configurations found.

Supplemental Figures

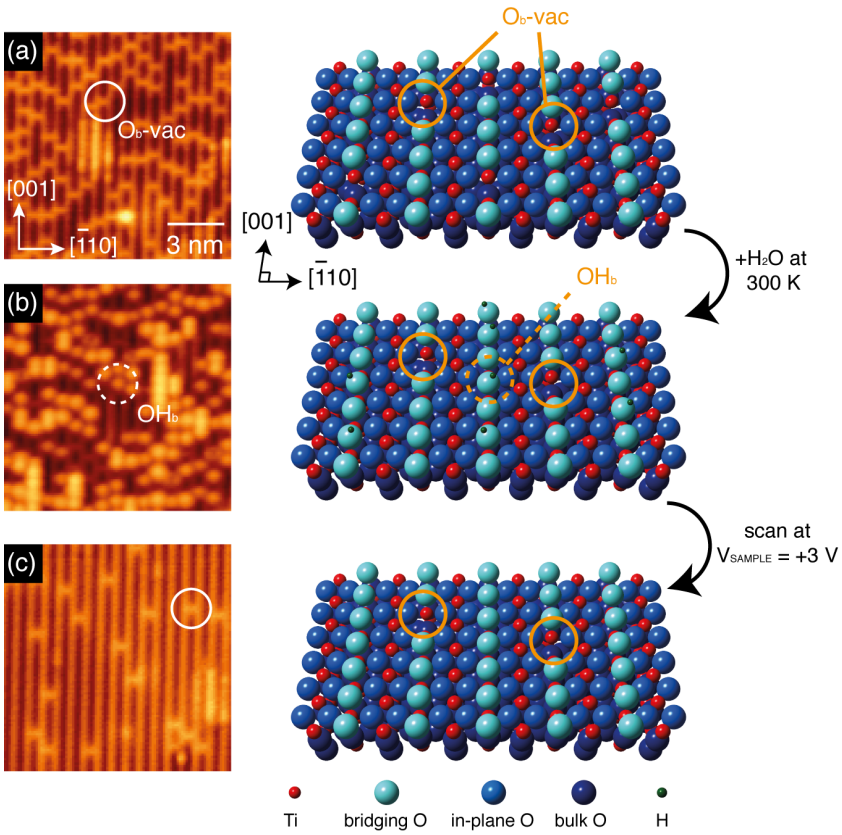

Figure S1: (a) STM image of as-prepared TiO_2(110) recorded at 78 K. Bright rows correspond to Ti_{5c} rows and dark rows to O_b rows. Solid circles mark O_b-vac′s that appear as protrusions along the O_b rows. (b) As (a), after exposing the surface to water from the residual vacuum at 300 K. This results in nearly all O_b-vacs reacting with the H_2O molecules, forming two OH_b per O_b-vac. (c) As (b), following a high voltage scan at sample bias of +3 V in STM. This removes all the capping H atoms of the OH_b species, leaving a small number of O_b-vacs on the surface. Schematics of rutile TiO_2(110) at the three sample conditions are shown on the right.

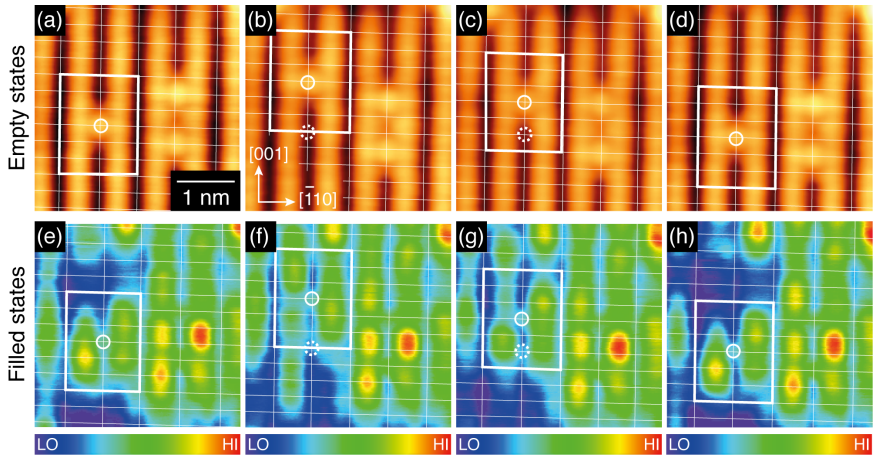

Figure S2: Simultaneously recorded empty- and filled- state STM images of the TiO_2(110) surface, taken before [panels (a), (e)] and after [panels (b)-(d), (f)-(h)] the manipulation of the position of a O_b-vac along [001] with voltage pulses (V_S = +4 V, 6 s). Solid (dashed) circles mark the current (initial) positions of the O_b-vacs. Rectangles are drawn around the O_b-vacs and mark the same areas between the empty- and filled-state images. Scanning parameters: V_S = +1 V, I_T = 10 pA for panels (a)-(d), V_S = -2 V, I_T = 0.3 pA for panels (e)-(h). The images were recorded at 7 K.

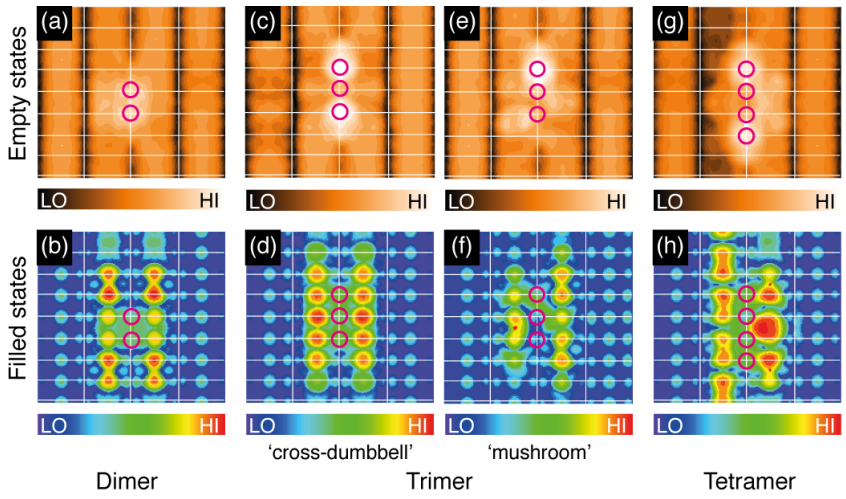

Figure S3. 4 × 8 unit cells simulated STM images of (a)-(b) the O_b-vac dimer, (c)-(d) 'cross-dumbbell' trimer, (e)-(f) 'mushroom' trimer, and (g)-(h) tetramer. The 'mushroom' trimer in panels (e)-(f) corresponds to that shown in Figs. 4(e)-(f), while the tetramer in panels (g)-(h) corresponds to that shown in Figs. 4(i)-(j). Intersections of the white grids mark the positions of O_b^{2-}. Circles mark the removed O_b^{2-}.

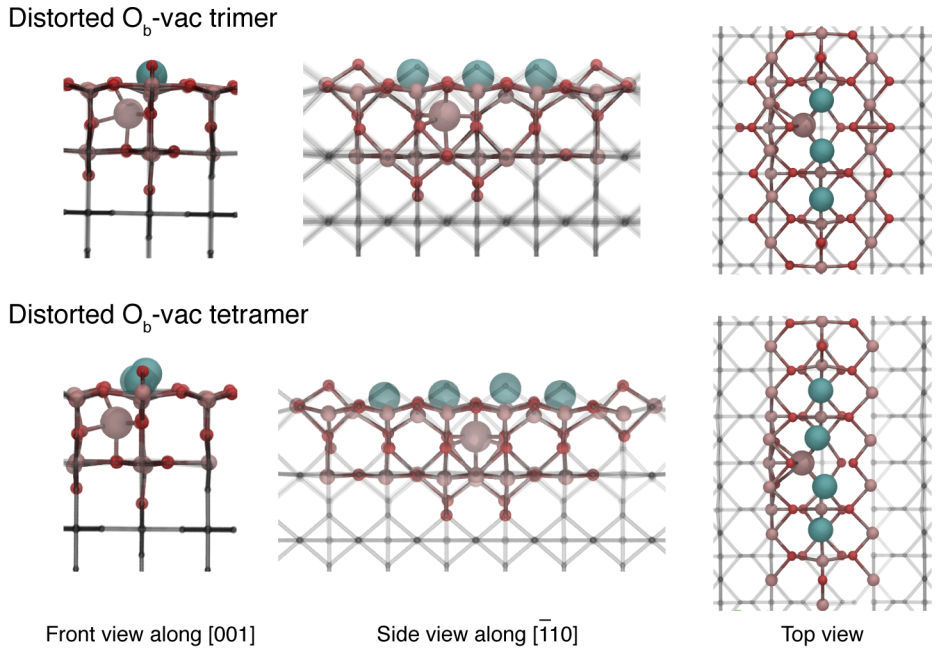

Figure S4: Atomic structures of the distorted O_b-vac trimer and tetramer as determined using classical molecular dynamics simulations. Turquoise spheres are sites of the removed bridging oxygen ions (O_b^{2-}). Large pink spheres are the Ti ions that are displaced to interstitial sites as a result of structural distortion. Small pink and red spheres are the Ti and O ions, respectively, in the O_b-vac complexes.

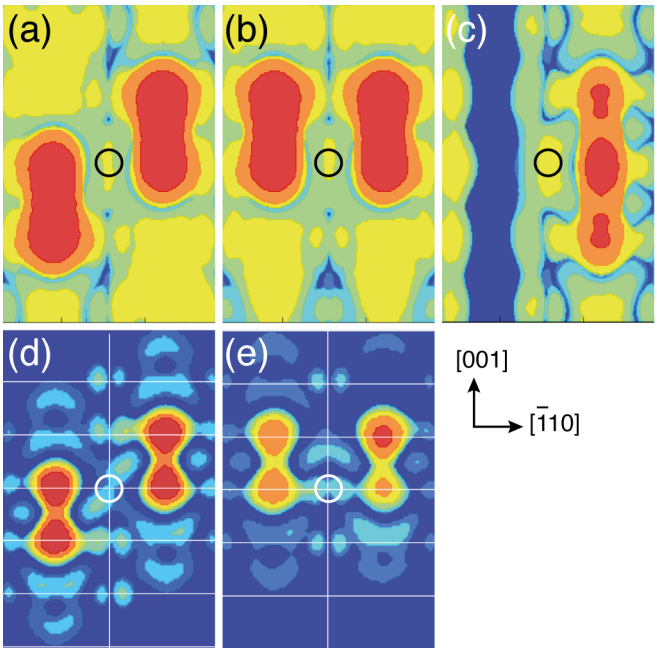

Figure S5: 2×6 unit-cell simulated filled state STM images of individual O_b-vacs obtained using (a)-(c) DFT+U plane-wave and (d)-(e) hybrid local basis set calculations. The equivalent configuration to that shown in panel (c) was not obtained in the hybrid local basis set calculations. Circles indicate the O_b-vac position.

Supplemental Movies

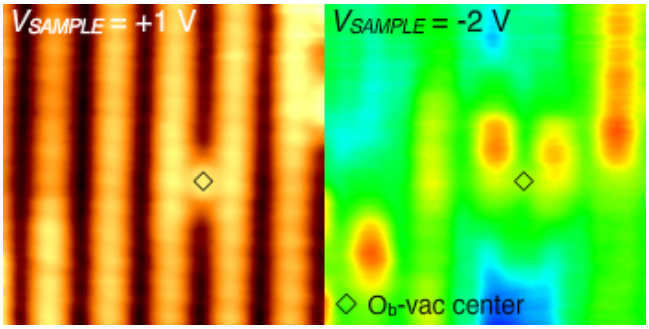

Movie S1: Displacement of a single O_b-vac of TiO_2(110) by STM tip pulses.

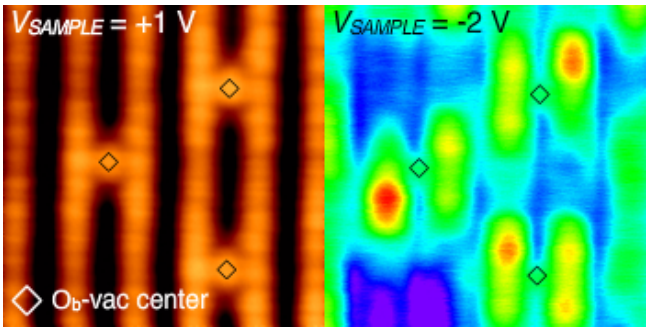

Movie S2: Separation of two neighboring O_b-vacs, followed by the formation of an O_b-vac dimer using tip pulses.

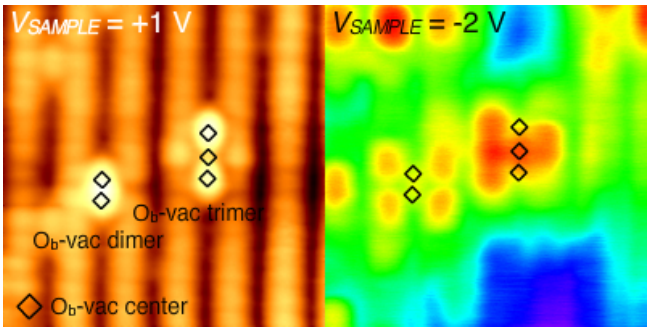

Movie S3: Formation of O_b-vac dimer and trimer using tip pulses.

References

[1] C. M. Yim, C. L. Pang, and G. Thornton, Phys. Rev. Lett. **104**, 036806 (2010).

[2] S. Wendt, R. Schaub, J. Matthiesen, E. K. Vestergaard, E. Wahlström, M. D. Rasmussen, P. Thostrup, L. M. Molina, E. Lægsgaard, I. Stensgaard, B. Hammer, and F. Besenbacher, Surf. Sci. **598**, 226 (2005).

[3] O. Bikondoa, C. L. Pang, R. Ithnin, C. A. Muryn, H. Onishi, and G. Thornton, Nat. Mater. **5**, 189 (2006).

[4] Z. Zhang, O. Bondarchuk, B. D. Kay, J. M. White, and Z. Dohnalek, J. Phys. Chem. B **110**, 21840 (2006).

[5] T. Minato, Y. Sainoo, Y. Kim, H. S. Kato, K.-I. Aika, M. Kawai, J. Zhao, H. Petek, T. Huang, W. He, B. Wang, Z. Wang, Y. Zhao, J. Yang, and J. G. Hou, J. Chem. Phys. **130**, 124502 (2009).

[6] S. Wendt, P. T. Sprunger, E. Lira, G. K. H. Madsen, Z. Li, J. O. Hansen, J. Matthiesen, A. Blekinge-Rasmussen, E. Lægsgaard, B. Hammer, and F. Besenbacher, Science **320**, 1755 (2008).

[7] C. L. Pang, O. Bikondoa, D. S. Humphrey, A. C. Papageorgiou, G. Cabailh, R. Ithnin, Q. Chen, C. A. Muryn, H. Onishi, and G. Thornton, Nanotechnology **17**, 5397 (2006).

[8] M. Batzill, K. Katsiev, D. J. Gaspar, and U. Diebold, Phys. Rev. B **66**, 235401 (2002).

[9] Y. Yoon, Y. Du, J. C. Garcia, Z. Zhu, Z.-T. Wang, N. G. Petrik, G. A. Kimmel, Z. Dohnálek, M. A. Henderson, R. Rousseau, N. A. Deskins, and I. Lyubinetsky, ChemPhysChem **16**, 313 (2015).

[10] K. Mitsuhara, H. Okumura, A. Visikovskiy, M. Takizawa, and Y. Kido, J. Chem. Phys. **136**, 124707 (2012).

[11] T. Minato, M. Kawai, and Y. Kim, J. Mater. Res. **27**, 2237 (2012).

[12] J. VandeVondele, M. Krack, F. Mohamed, M. Parrinello, T. Chassaing, and J. Hutter, Comput. Phys. Commun. **167**, 103 (2005).

[13] M. Guidon, J. Hutter, and J. VandeVondele, J. Chem. Theory Comput. **5**, 3010 (2009).

[14] M. Guidon, J. Hutter, and J. VandeVondele, J. Chem. Theory Comput. **6**, 2348 (2010).

[15] J. VandeVondele and J. Hutter, J. Chem. Phys. **127**, 114105 (2007).

[16] C. Hartwigsen, S. Goedecker, and J. Hutter, Phys. Rev. B **58**, 3641 (1998).

[17] M. Krack, Theor. Chem. Acc. **114**, 145 (2005).

[18] J. VandeVondele and J. Hutter, J. Chem. Phys. **118**, 4365 (2003).

[19] C. Di Valentin, J. Chem. Phys. **127**, 154705 (2007).

[20] L. Genovese, T. Deutsch, and S. Goedecker, J. Chem. Phys. **127**, 054704 (2007).

[21] G. Henkelman, B. P. Uberuaga, and H. Jónsson, J. Chem. Phys. **113**, 9901 (2000).

[22] J. B G Dick and A. W. Overhauser, Physical Review **112**, 90 (1958).

[23] M. Matsui and M. Akaogi, Mol. Simul. **6**, 239 (1991).

[24] S. Kerisit, N. A. Deskins, K. M. Rosso, and M. Dupuis, J. Phys. Chem. C **112**, 7678 (2008).

[25] G. Bussi, D. Donadio, and M. Parrinello, J. Chem. Phys. **126**, 014101 (2007).

[26] J. Tersoff and D. Hamann, Phys. Rev. B **31**, 805 (1985).